Submitted to the ASCE *Journal of Engineering Mechanics*, 2002.

THE PHASE I IASC-ASCE STRUCTURAL HEALTH MONITORING BENCHMARK PROBLEM USING SIMULATED DATA

E.A. Johnson,[*1] Assoc. M. ASCE, H.F. Lam,[2] L.S. Katafygiotis,[3] Assoc. M. ASCE, and J.L. Beck,[4] M. ASCE

ABSTRACT: Structural health monitoring (SHM) is a promising field with widespread application in civil engineering. SHM has the potential to make structures safer by observing both long-term structural changes and immediate post-disaster damage. However, the many SHM studies in the literature apply different monitoring methods to different structures, making side-by-side comparison of the methods difficult. This paper details the first phase in a benchmark SHM problem organized under the auspices of the IASC-ASCE Structural Health Monitoring Task Group. The scale-model structure adopted for use in this benchmark problem is described. Then, two analytical models based on the structure — one a 12DOF shear-building model, the other a 120DOF model, both finite-element based — are given. The damage patterns to be identified are listed as well as the types and number of sensors, magnitude of sensor noise, and so forth. MATLAB® computer codes to generate the response data for the various cases are explained. The codes, as well as details of the ongoing Task Group activities, are available on the Task Group web site at http://wusceel.cive.wustl.edu/asce.shm/ .

Key words: structural health monitoring, damage detection, benchmark problems, civil structures

INTRODUCTION

Structural health monitoring (SHM) systems seek to monitor the state of a structure's "health" — that is, to determine the level and location of damage or deterioration within a structure. Chang (1999) defined SHM as an "autonomous [system] for the continuous monitoring, inspection, and damage detection of [a structure] with minimum labor involvement." SHM has

* Corresponding author.
1. Asst. Prof., Dept. of Civil Engrg., Univ. of Southern California, Los Angeles, CA 90089. JohnsonE@usc.edu
2. Demonstrator, Dept. Civil Engrg., Hong Kong Univ. of Sci. & Tech., Clear Water Bay, Kowloon, Hong Kong. paullam@ust.hk
3. Asst. Prof., Dept. Civil Engrg., Hong Kong Univ. of Sci. and Tech., Clear Water Bay, Kowloon, Hong Kong. lambros@ust.hk
4. Professor, Div. of Engrg. and Appl. Sci., California Institute of Technology, Pasadena, CA 91125. jimbeck@caltech.edu

application for all types of structures. For civil engineering purposes, detecting the acute damage caused by earthquakes immediately after the event or monitoring the long-term deterioration due to the environment and human use (and abuse) can provide vital information on structural safety. Such information can then be used to assess and plan future use and repairs, as well as estimate changes in the expected lifetime of the structure.

Benefits of Structural Health Monitoring and Damage Detection (SHM/DD)

Recent seismic disasters, including those in the past several years in Turkey, Taiwan and India, demonstrated yet again the damage caused by earthquakes that occur in or near urban areas. Though the magnitude 6.8 Nisqually earthquake near Seattle in February 2001 did not cause severe widespread damage — $1 to $2 billion cost — it served to remind us again of the continued need to be prepared for future seismic events. The level of structural damage caused by an earthquake is sometimes immediately obvious (*e.g.*, a building that has toppled over), but damage is often hidden within a structure, such as damaged joints embedded behind walls or encased in concrete. Such damage is difficult and expensive to discover by visual inspection, but may still pose a risk to the health and integrity of the structure. For example, significant expenditures after the 1994 Northridge earthquake went to inspecting joints of steel structures for damage, requiring extensive removal of non-structural material, not to mention putting (at least part of) the structure out of service during inspection. Similar expenditures were required after the 1995 Great Hanshin (Hyogo-Ken Nanbu or Kobe) earthquake as well (Mita, 1999). SHM systems may prove invaluable in future urban earthquakes by giving quick assessments of the damage level of a structure shortly after the quake itself. Not only would this give the structure owner knowledge of what and

where damage may have occurred, but also whether immediate actions are necessary to evacuate building occupants or contents or to reroute around damaged highways or bridges.

The benefits of monitoring long-term structural integrity are also dramatic. The costs of civil infrastructure maintenance, repair, and replacement are extensive — total construction costs are estimated at about 10% of GDP for most major industrialized nations. Further, many civil structures in the U.S. and abroad are now, or will soon be, approaching their design lives or are already considered substandard (*e.g.*, Danhausen, 1995; Helmicki *et al.*, 1999; Rahman *et al.*, 1999). The dominant method today for evaluating the integrity of civil structures is manual, visual inspection — a time-intensive and costly procedure. Further, scheduling timely repair and maintenance is difficult. An autonomous structural health monitoring system has the potential to eliminate the costs of regular periodic inspections, and to more accurately determine the condition of a deteriorating structure so as to better estimate remaining life and the upgrades necessary to keep the structure sufficiently safe. Further, a monitoring system can help avoid many unexpected failures that may lead to economic or personal injury.

Currently, acquisition of sensor information is not a crucial issue. Several recent workshops and symposia on SHM and Damage Detection (*e.g.*, Chang, 1997, 1999, 2001) have demonstrated significant developments in sensor technologies for a variety of monitoring purposes. However, the authors' impressions of these meetings, which have been echoed by other SHM researchers, have been that the critical problem now is not the acquisition of information. Clearly, collecting terabytes of data from a single structure is well within the capabilities of today's hardware and software. Rather, crucial algorithmic developments are needed to process the vast wealth of information and provide useful and simple measures of a structure's current health status.

SHM Benchmark Studies and the IASC-ASCE SHM Task Group

There have been numerous studies by researchers around the world applying various SHM techniques. The interested reader is directed particularly to the extensive review papers by Doebling *et al.* (1996, 1998). SHM systems may be classified in various ways. One way is local versus global methods. Local SHM methods detect changes in a structure in localized regions; some examples are various ultrasonic and x-ray devices, and piezoelectric devices (*e.g.*, Park *et al.*, 1999a,b)). Global SHM methods — sometimes called vibration-based methods — may be further classified by using unmeasured (and, often, unmeasurable) ambient excitation or known (or measurable) excitation. The former, of course, requires no artificial excitation source and is, thus, simpler from an implementation point of view. Examples of ambient excitation are microtremors, wind, traffic, waves, mechanical processes, human factors, etc. Known excitation SHM methods for civil structures have focused on using actuators of various kinds, including impact devices, step-relaxation methods (*e.g.*, releasing a tensioned cable), and shakers (rotating unbalanced devices, servo-hydraulic devices, or electrodynamic devices). (A brief review of excitation for bridges is given by Farrar *et al.* (1999).)

A difficulty, however, is that the various studies apply different SHM/DD methods to different structures, rendering side-by-side comparison difficult. A benchmark study, where participants apply a number of monitoring techniques to a common structure with common objectives, provides a platform for consistent evaluation of the proposed SHM methods. One such recent benchmark study was initiated at the *15th International Modal Analysis Conference* (IMAC XV) and is detailed in Black and Ventura (1998). This study was a "blind test" in that the participants were provided with forced vibration response data of a scale-model steel frame structure in

undamaged and damaged (certain elements removed from the frame) states but with no knowledge of the level or location(s) of damage. The task, then, was to identify where the damage had occurred. The blind test is, of course, a realistic measure of the performance of different SHM methods. However, it makes it difficult for researchers to understand the advantages and disadvantages of the methods, particularly the sensitivity to various aspects of the problem, such as full or limited sensor information, the effects of noise, and so forth. In the end, only one paper was actually submitted to the next IMAC conference directly addressing this blind test (Park *et al.*, 1998). Presumably, researchers were a bit leery of the completely blind nature of the study.

At the 1996 International Workshop on Structural Control (Chen, 1996), a plan was formed by the International Association for Structural Control (IASC) to create task groups to study the problem of structural health monitoring with particular focus on civil structures. Three task groups — one per region (Europe, Asia, U.S.) — were to be formed. The U.S. task group solidified in 1999 jointly under the auspices of the U.S. Panel on Structural Control (1990) and of the Dynamics committee of the ASCE Engineering Mechanics Division with Prof. James L. Beck (Caltech) as chair. Prof. Dennis Bernal took over as chair March 2001 until early 2003. This joint IASC-ASCE task group met first in June 1999 at the *13th ASCE Engineering Mechanics Conference* at Johns Hopkins University, and has had regular subsequent working meetings (Caltech, August 1999; USC, February 2000; UT-Austin [EM2000], May 2000; WashU, September 2000; Caltech, March 2001; San Diego [MMC2001], June 2001; Como, Italy, April 2002; a planned meeting at Stanford [3IWSHM] on 12 September 2001 did not materialize for obvious reasons). The task group is charged with studying the efficacy of various structural health monitoring methods.

The IASC-ASCE SHM Task Group is developing a series of benchmark SHM problems, beginning with a relatively simple problem and proceeding on to more realistic (but more difficult) problems. This paper details the first phase of this study, based on simulated response of a test structure that forms the cornerstone of the work. The motivation for the structural model is discussed, as well as the data generation mechanisms for the simulated data. Subsequent papers in this journal issue will apply several SHM/DD methods to this common benchmark problem. Later work will involve analysis of experimental data from the test structure.

SHM/DD BENCHMARK PROBLEM DEFINITION

The Benchmark Structure

The Task Group decided that the use of simulated data from an analytical structural model based on an existing structure would allow for future comparisons with data taken on the actual structure. Starting with simulated data allows participants to better understand the sensitivities of their methods to various aspects of the problem, such as difference between the identification model and the true model, incomplete sensor information, and the presence of noise in measurement signals. Since the earlier "blind test" study was based on data from a scale-model structure, the Task Group chose to use an analytical model based on the same structure.

The structure (Black and Ventura, 1998), shown in Fig. 1, is a 4-story, 2-bay by 2-bay steel-frame scale-model structure in the Earthquake Engineering Research Laboratory at the University of British Columbia (UBC). It has a 2.5 m $\times$ 2.5 m plan and is 3.6 m tall. The members are hot rolled grade 300W steel with a nominal yield stress 300 MPa (42.6 kpsi). The sections are unusual, designed for a scale model, with properties as given in Table 1. The columns are all ori-

ented to be stronger bending toward the x-direction (*i.e.*, about the y-axis). The floor beams are oriented to be stronger bending vertically, *i.e.*, about the y-axis (x-axis) for those oriented with longitudinal axis parallel to the x-axis (y-axis). The braces have no bending stiffness, so their orientation is irrelevant. There is one floor slab per bay per floor: four 800 kg slabs at the first level, four 600 kg slabs at each of the second and third levels, and, on the fourth floor, either four 400 kg slabs or three 400 kg and one 550 kg to create some asymmetry (discussed further below).

Two finite element models based on this structure were developed to generate the simulated response data. The first is a 12DOF shear-building model that constrains all motion except two horizontal translations and one rotation per floor. The second is a 120DOF model that only requires floor nodes have the same horizontal translation and in-plane rotation. The columns and floor beams are modeled as Euler-Bernoulli beams in both finite element models. The braces are bars with no bending stiffness. A diagram of the analytical model is shown in Fig. 2. Note the x-direction (*i.e.*, bending about the y-axis) is the strong direction due to the orientation of the columns. Further, to be consistent with the axes used in later experimental tests (Dyke *et al.*, 2001), the compass directions associated with the axes are South for the positive y (weak) direction, and West for the positive x (strong) direction.

Damage Patterns

In addition to the undamaged structure, six damage patterns are studied as a part of the benchmark problem. These damage patterns advance from simple extreme damage that most any method should be able to detect, to more difficult cases. The damage patterns are not intended to directly represent the complexity of damage mechanisms, but will test the ability of various

SHM/DD methods in detecting, localizing, and quantifying damage. The damage patterns are shown graphically in Fig. 3, and are defined as follows:

(*i*) no stiffness in the braces of the first story (*i.e.*, the braces still contribute mass, but provide no resistance within the structure),

(*ii*) no stiffness in any of the braces of the first and third stories,

(*iii*) no stiffness in one brace in the first story (north brace on the west face of the structure; noted with the ellipse in Fig. 3*iii*),

(*iv*) no stiffness in one brace in the first story (north brace on the west face) and in one brace in the third story (west brace on the north face),

(*v*) the same as damage pattern (*iv*) but with the north floor beam at the first level on the west face of the structure (*i.e.*, the beam from ((2.5m, 0, 0.9m) to (2.5m, 1.25m, 0.9m)) partially unscrewed from the northwest column at (2.5m, 0, 0.9m) — consequently, the beam-column connection there can only transmit forces and cannot sustain any bending moments — and

(*vi*) two-thirds stiffness (*i.e.*, a one-third stiffness loss) in one brace in the first story (the same brace damaged in pattern (*iii*): the north brace on the west face).

12DOF Shear-Building Model

Two finite element models of the structure were developed to generate the simulated data for the SHM/DD benchmark problem in the undamaged and damaged conditions. The first finite element model is a twelve degree-of-freedom (12DOF) shear building model. In this model, the floors (floor beams and floor slabs) move as rigid bodies, with translation in the x- and y-directions and rotation θ about the center column. Thus, there are three degrees-of-freedom per floor. The

columns are modeled as linear elastic Euler-Bernoulli beams, and the braces as axial bars. A MATLAB® based finite element analysis code (available through the Task Group web site http://wusceel.cive.wustl.edu/asce.shm/) is used to compute mass **M** and stiffness **K** matrices. The natural frequencies are given in Table 2 for the undamaged structure and for damage patterns (*i*) and (*ii*). The mode shapes of the first three modes are shown in Fig. 4. The model has story stiffnesses as shown in Table 3, with percent loss of story stiffnesses for each damage pattern shown in Table 4, and the 12DOF stiffness matrix **K** is given in the Appendix. Note that since the floor is perfectly rigid and bending of the floor beams is not allowed, damage pattern (*v*) is no different than (*iv*) for the 12DOF model (this will not be the case for the 120DOF model as shown below). As discussed previously, some of the cases to be studied have some asymmetry in the mass of the fourth floor; the natural frequencies of the lumped-mass 12DOF model with this asymmetry are shown in Table 5.

In fact, two 12DOF models have been studied as a part of this benchmark problem. The initial code, developed by the first author and denoted herein as the *USC code*, used a consistent mass matrix, but neglected any mass of damaged braces and is restricted to a unidirectional study and the first two damage patterns (cases 1 and 2 as defined below). The later code, spearheaded by the second author and discussed in more depth below, incorporated the options to study the more complex 120DOF data generation model and the more advanced cases and damage patterns, but used a lumped mass matrix (and includes the mass from damaged braces) — this code is denoted the *HKUST code*. However, the consistent mass matrix in the initial *USC code* allows for identification model error. Further, some of the application papers to follow report their initial results identifying damage in this structure with the consistent mass matrix. Consequently, the natural frequencies are given in Table 2 for both lumped (*HKUST code*) and consistent (*USC code*) mass

matrices, and both matrices are given in the Appendix. However, for ease of use, consistency, and study of the advanced cases, the later *HKUST code* should be used for any new studies of this problem.

120DOF Model

Most structures are not as simple as engineers often model them, which leads to the presence of model error. To include model error effects in this benchmark study, a more complex 120DOF model was constructed using finite elements. This model is used to simulate the response measurements, while the model used in the identification analyses remains the (simpler) 12DOF shear-building model. The 120DOF model constrains the horizontal translation and rotation (about the vertical axis) of the nodes in each floor to be the same. The horizontal slab panels are assumed to contribute only towards the in-plane stiffness making the floor behave as rigid with respect to in-plane motions only. The remaining out-of-plane degrees of freedom (namely, vertical motion and pitching/rolling of the floor) are active. The resulting natural frequencies, given in Table 2 for undamaged and damage patterns (*i*) and (*ii*) with symmetric mass and in Table 6 for all damage patterns with asymmetric mass, are lower than those of the 12DOF case due to fewer constraints. (Some participants in this study may have used an older version of the *HKUST code* that had a different orientation for the floor beams, resulting in slightly lower natural frequencies; those natural frequencies were reported in previous conference papers (Johnson *et al.*, 2000, 2001, 2002)).

"Equivalent" horizontal story stiffnesses do not have a unique definition. One possible approach is to look just at the elements of the 120DOF stiffness matrix that are in rows and columns corresponding to the horizontal (x, y, and θ) degrees of freedom. This results in a reduced stiffness matrix that gives story stiffnesses identical to those for the 12DOF model given in

Table 3. Another approach is to define the "equivalent" stiffness based on the effects of a unit force applied to each of the 12 degrees-of-freedom on the induced motion in those same degrees-of-freedom. This reduces to finding a 12DOF shear-building stiffness matrix whose inverse — the flexibility matrix — is close to the corresponding rows and columns of the 120DOF flexibility matrix. A least-squares optimization may be used to find this "equivalent" 12DOF model, and the resulting story stiffnesses. This approach results in the story stiffnesses given in Table 7 and percent loss of story stiffnesses for each damage pattern given in Table 8. Because of the coupling of vertical and horizontal motion, removing braces affects the "equivalent" horizontal stiffness on floors above and below where the brace was actually removed.

Time History Response Simulation Cases

The finite element models (either the 12 or 120 DOF models) give a structural model in terms of active degrees of freedom $\mathbf{q}$, related to physical degrees of freedom by $\mathbf{x} = \mathbf{T}\mathbf{q}$. The equation of motion is $\mathbf{M}\ddot{\mathbf{q}} + \mathbf{C}_d\dot{\mathbf{q}} + \mathbf{K}\mathbf{q} = \mathbf{T}^T\mathbf{f}$ where $\mathbf{f}$ = a vector of forces applied to the physical degrees of freedom. Sixteen accelerometers, two each in the *x*- and *y*-directions per floor, return noisy sensor measurements: $\ddot{\mathbf{y}} = \mathbf{C}\mathbf{q} + \mathbf{D}\mathbf{f} + \mathbf{v}$ where $\mathbf{v}$ = a sensor noise vector, the elements of which are Gaussian pulse processes with RMS 10% of the largest RMS of the acceleration responses (typically one of the roof accelerations). 1% modal damping is assumed in each mode, so $\mathbf{C}_d$ is computed based on the solution to the standard $\mathbf{K}\boldsymbol{\Phi} = \mathbf{M}\boldsymbol{\Phi}\boldsymbol{\Lambda}$ eigenvalue problem. Two sets of excitations are used in various cases of the benchmark problem: independent loading in the *y*-direction at each floor as in Fig. 5; or as a roof acceleration at the center column in a direction $\pm(\hat{\mathbf{i}} - \hat{\mathbf{j}})$ (where $\hat{\mathbf{i}}$ and $\hat{\mathbf{j}}$ are unit vectors in the *x*- and *y*-directions, respectively). In both loading

scenarios, the excitation(s) are modeled as independent filtered Gaussian white noise (Gaussian white noise processes passed through a 6^{th} order low-pass Butterworth filter with a 100 Hz cutoff).

Two methods of time history integration are given as options to the user. The first uses MATLAB's *lsim* command, which uses a discrete-time integration algorithm that assumes excitation is constant over a time step. The other integration algorithm uses the Nigam-Jennings integration that decomposes the system into modal space, integrates each mode assuming the excitation is piecewise linear over a time step, and superimposes to get the time response (Nigam and Jennings, 1968, 1969). The nominal integration time step should be 0.001 seconds, to a duration of about 100 seconds. Participants in the benchmark study are free to adjust these, but must justify significant deviations. The acceleration time history responses are available, then, at a 1 kHz sampling rate but participants may freely use lower sampling rates as they wish (to reduce computational effort, for example). Sample time histories for several cases and damage patterns are shown in Fig. 6, and the corresponding power spectral densities, that expose the modes of the system, are shown in Fig. 7.

A total of six cases are defined as a part of this phase 1 benchmark problem, each with several components including the various damage patterns. The matrix of simulation cases is shown in Table 9. Figure 5 depicts the scenario for the first two simulation cases, which is a one-dimensional analysis in the weak (y) direction. The excitations are applied one per floor as approximating wind or other ambient excitation, and are modeled as independent filtered Gaussian white noise. Subsequent cases add additional realism (though not yet to the stage of the complexity of a full-scale structure). Case 3 replaces the "ambient" excitation with a shaker on the roof (top of the center column). Although the structure is excited in two directions, only the y-direction is to be

analyzed for Case 3. Cases 4–6 introduce asymmetry by replacing one of the 400 kg floor slabs on the roof (the one with hatched shading in Fig. 5) with a 550 kg slab, and are analyzed with 3-D motion of the floors. Case 4 reverts to the 12DOF data generation model, but case 5 brings model error back into the picture and introduces damage pattern (v). Case 6 decreases the number of sensors by 50% to test the ability of various SHM/DD algorithms to be robust to limited sensor data.

Data Generation Program: datagen

The data generation program for this phase 1 benchmark problem is available on the Task Group web site http://wusceel.cive.wustl.edu/asce.shm/ . This MATLAB program, called *datagen*, provides both command-line and graphical user interface (GUI) methods of building the 12 or 120 DOF finite element models and simulating their response. The resulting acceleration time histories (as well as other parameters like the mass and stiffness matrices) are stored in a MATLAB .mat file, and can be loaded into MATLAB for analysis by the identification, monitoring, or damage detection code of interest. The GUI has four primary modal windows that sequentially request user input. Snapshots of these GUIs are shown in Fig. 8. The first GUI (Fig. 8*a*) asks the user which case for which it should generate the date. The second (Fig. 8*b*) asks what damage pattern should be used. The third (Fig. 8*c*) asks the user to select the integration scheme for simulating the response time histories. And finally, the fourth (Fig. 8*d*) asks for the numerical values of a number of parameters. Default values are provided, some of which are prescribed as part of the benchmark definition (but the user can change them if it helps demonstrate some aspect of their identification or damage detection methodology). Most of these are described above or are self-explanatory. The "noise level" is the RMS of the sensor noises, generated using independent Gaussian pulse processes, as a percentage of the maximum RMS acceleration responses; this noise

level should be 10% for the benchmark problem. The "filter index" is a boolean value (0 or 1) indicating whether the excitation(s) should be passed through the aforementioned low-pass filter; this option is included because the Butterworth filter requires the Signal Processing toolbox in MATLAB, which may not be available for all interested parties. The "formal" benchmark definition uses this filter so that the excitation and responses have finite variances that do not depend on the length of the time step. The random number generator seed can be adjusted to give different excitation and noise time histories to perform multiple analyses. Finally, the name of the output .mat datafile may be chosen.

While not a part of the formal benchmark definition, the GUI provides a means for selecting and defining an arbitrary damage pattern. Clicking on "User define damage case" in Fig. 8*b* causes *datagen* to pop up a list of element categories (Fig. 9*a*) and a frame drawing of the structure with elements numbered (Fig. 9*b*). Selecting one of the element categories brings up another window to choose specific elements that are damaged (Fig. 9*c*). The element, if checked, is assumed to lose all of its stiffness.

CONCLUSIONS

An autonomous monitoring system that has the capability of predicting what parts of a structure are damaged and which are not would have a positive economic impact, as well as the potential for saving lives by giving quick assessments of structural health to indicate whether continued use of a structure may be allowed or if alternate routes must be used by emergency vehicles and other necessary traffic. Quick and effective prioritization of actions after a seismic disaster is infeasible with manual inspection. However, a number of autonomous health monitoring methods

have been studied and tested in recent years. While promising, it is often difficult to compare the merits of various approaches as they are typically applied to different structures, with different excitation models, and evaluated on different criteria. A benchmark study can help provide a common basis for studying and exploring a variety of health monitoring and damage detection approaches. Further, rooting a benchmark in a modern programming language like MATLAB helps simplify and make transparent the modelling and response calculations in an open code; further, users can modify the code as needed to fit the peculiarities of their chosen SHM/DD methodology.

This paper has detailed the first phase of a benchmark problem in structural health monitoring. The benchmark problem is based on simulated response time histories of a laboratory-scale frame building. 12 and 120 DOF finite element models are used to generate the response data. Participants are charged with using a 12DOF shear-building as their identification model. Six cases are defined with undamaged and six damage patterns. The IASC-ASCE Task Group on Structural Health Monitoring has been studying this phase of the benchmark problem, and the remainder of the papers in this special journal issue apply various SHM methods to this phase of the benchmark problem. The Task Group encourages participation in this benchmark study by researchers around the world and would appreciate any comments or suggestions on this work. More details on this study, as well as the current and future efforts of the Task Group, are available on the web at http://wusceel.cive.wustl.edu/asce.shm/ .

ACKNOWLEDGMENTS

The authors wish to thank the other members of the IASC-ASCE SHM Task Group for their assistance, suggestions, and cooperation in the development of this benchmark problem, particu-

larly: Dionisio Bernal (Northeastern Univ.), Raimondo Betti (Columbia Univ.), Joel P. Conte (UCLA), Shirley J. Dyke (Wash. Univ. St. Louis), Sami F. Masri (Univ. of Southern California), Andrew Smyth (Columbia Univ.), and Carlos E. Ventura (Univ. of British Columbia). Thanks especially to Prof. Ventura for the photograph and the properties of the UBC frame, and to Prof. Conte for assistance in calibrating the finite element models described herein.

The authors gratefully acknowledge the partial support of this research by the National Science Foundation under CAREER grant CMS 00-94030.

APPENDIX. MASS AND STIFFNESS MATRICES FOR 12DOF MODELS

Some methods of health monitoring may require knowledge, partial or full, of the mass matrix of the structure. As participants of this benchmark problem are to use a 12DOF shear-building identification model, the mass matrices for the 12DOF models are given in Fig. 10. Further, for purposes of comparison with participant results, the stiffness matrices of the 12DOF models in undamaged and in the 6 damage cases, are shown in Fig. 11.

APPENDIX. REFERENCES

Black, C.J., and C.E. Ventura (1998). "Blind Test on Damage Detection of a Steel Frame Structure." *16th International Modal Analysis Conference* (IMAC XVI), Santa Barbara, California, February 2–5, 1998. Proceedings, 623–629.

Chang, F.-K. (1997). *Structural Health Monitoring: Current Status and Perspectives*, Proceedings of the International Workshop on Structural Health Monitoring, Stanford University, September 18–20, 1997, Technomic Publishing Co., Lancaster, PA.

Chang, F.-K. (1999). *Structural Health Monitoring 2000,* Proceedings of the 2nd International Workshop on Structural Health Monitoring, Stanford University, September 8–10, 1999, Technomic Publishing Co., Lancaster, PA.

Chang, F.-K. (2001). *Structural Health Monitoring,* Proceedings of the 3nd International Workshop on Structural Health Monitoring, Stanford University, September 12–14, 2001.

Chen, J.C., ed. (1996). *Proceedings of the Second International Workshop on Structural Control: Next Generation of Intelligent Structures*, Hong Kong, December 18–21, 1996. Available on the web pages of the *US Panel on Structural Control Research* http://cwis.usc.edu/dept/civil_eng/structural/welcome.html .

Danhausen, W.O. (1995). *Better Roads*, **65**(11), 26.

Doebling, S.W., C.R. Farrar, M.B. Prime, and D.W. Shevitz (1996). "Damage Identification and Health Monitoring of Structural and Mechanical Systems from Changes in their Vibration Characteristics: A Literature Review." Los Alamos National Laboratory Report, LA-13070-MS (http://www.lanl.gov/projects/ncsd/pubs/lit_review.pdf).

Doebling, S.W., C.R. Farrar, and M.B. Prime (1998). "A Summary Review of Vibration-Based Damage Identification Methods." *The Shock and Vibration Digest*, **30**(2), 91–105.

Dyke, S.J., D. Bernal, J.L. Beck, and C. Ventura (2001). "An Experimental Benchmark Problem in Structural Health Monitoring." *Structural Health Monitoring,* Proceedings of the 3nd International Workshop on Structural Health Monitoring, Stanford University, September 12–14, 2001.

Farrar, C.R., T.A. Duffey, P.J. Cornwell, and S.W. Doebling (1999). "Excitation Methods for Bridge Structures." *17th International Modal Analysis Conference (IMAC XVII)*, Kissimmee, Florida, February 8–11, 1999. Proceedings (Society for Experimental Mechanics, Bethel, Connecticut, 1999), 1063–1068.

Helmicki, A., V. Hunt, M. Shell, M. Lenett, A. Turer, V. Dalal, and A. Aktan (1999). "Multidimensional Performance Monitoring of a Recently Constructed Steel-Stringer Bridge." *Structural Health Monitoring 2000* (F.-K. Chang, ed.), Technomic Publishing Co., 408–416.

Johnson, E.A., H.F. Lam, L.S. Katafygiotis, and J.L. Beck (2000). "A Benchmark Problem for Structural Health Monitoring and Damage Detection." *14th ASCE Engineering Mechanics Conference (EM2000)*, Austin, Texas, May 21–24, 2000. CD-ROM Proceedings (J.L. Tassoulas, ed.), paper EAJOHN.PDF, 6 pages.

Johnson, E.A., H.F. Lam, L.S. Katafygiotis, and J.L. Beck (2001). "A Benchmark Problem for Structural Health Monitoring and Damage Detection." In F. Casciati and G. Magonette (eds.), *Structural Control for Civil and Infrastructure Engineering*, World Scientific, Singapore, 317–324.

Johnson, E.A., H.F. Lam, L.S. Katafygiotis, and J.L. Beck (2002). "A Simulated Data Benchmark Problem in Structural Health Monitoring." In F.-K. Chang (ed.), *Structural Health Monitoring: the Demands and Challenges*, CRC Press, New York, 469–477.

Mita, A. (1999). "Emerging Needs in Japan for Health Monitoring Technologies in Civil and Building Structures." *Structural Health Monitoring 2000* (F.-K. Chang, ed.), Technomic Publishing Co., 56–67.

Nigam, N.C., and P.C. Jennings (1968). "Digital calculation of Response Spectra from Strong-Motion Earthquake Records," Earthquake Engineering Research Laboratory technical report, California Institute of Technology, Pasadena, CA. Available online at http://resolver.library.caltech.edu/caltechEERL:1968.EERL.1968.002 .

Nigam, N.C., and P.C. Jennings (1969). "Calculation of response spectra from strong-motion earthquake records, Bulletin of the Seismological Soceity of America, **59**, 909–922.

Park, G., H. Cudney, and D.J. Inman (1999a). "Developing a Model Based Health Monitoring Technique using Structural Impedance Sensors." *Proceedings, 2nd International Conference on Identification in Engineering Systems*, University of Wales, Swansea, United Kingdom, March 29–31, 1999, 506–515.

Park, G., H.H. Cudney, and D.J. Inman (1999b). "Impedance-Based Health Monitoring Technique for Civil Structures." *Structural Health Monitoring 2000* (F.-K. Chang, ed.), Technomic Publishing Co., 523–532.

Park, S., N. Stubbs and R.W. Bolton (1998). "Damage Detection on a Steel Frame Using Simulated Modal Data." *16th International Modal Analysis Conference* (IMAC XVI), Santa Barbara, California, February 2–5, 1998. Proceedings, 612–622.

Rahman, M.S., T. Oshima, S. Mikami, T. Yamazaki, and I. Tamba (1999). "Diagnosis of Aged Bridge by Using Intelligent Monitoring System." *Structural Health Monitoring 2000* (F.-K. Chang, ed.), Technomic Publishing Co., 484–493.

U.S. Panel on Structural Control (1990). Web site http://www.usc.edu/dept/civil_eng/structural/welcome.html .

Property		*Columns*	*Floor Beams*	*Braces*
section type		B100×9	S75×11	L25×25×3
cross-sectional area	A [m^2]	1.133×10^{-3}	1.43×10^{-3}	0.141×10^{-3}
moment of inertia (strong direction)	I_y [m^4]	1.97×10^{-6}	1.22×10^{-6}	0
moment of inertia (weak direction)	I_z [m^4]	$.664\times10^{-6}$	$.249\times10^{-6}$	0
St. Venant torsion constant	J [m^4]	8.01×10^{-9}	38.2×10^{-9}	0
Young's Modulus	E [Pa]	2×10^{11}	2×10^{11}	2×10^{11}
Shear Modulus	G [Pa]	E / 2.6	E / 2.6	E / 2.6
Mass per unit volume	ρ [kg/m^3]	7800	7800	7800

Table 1: Properties of structural members.

Undamaged			*Damage Pattern (i)* no 1st floor braces			*Damage Pattern (ii)* no 1st & 3rd floor braces		
12DOF consistent mass	*12DOF* lumped mass	*120DOF* lumped mass	*12DOF* consistent mass	*12DOF* lumped mass	*120DOF* lumped mass	*12DOF* consistent mass	*12DOF* lumped mass	*120DOF* lumped mass
9.41 y	9.41 y	8.59 y	6.24 y	6.24 y	5.47 y	5.83 y	5.82 y	4.96 y
11.79 x	11.79 x	9.18 x	9.91 x	9.91 x	7.37 x	9.52 x	9.51 x	6.68 x
16.53 θ	16.38 θ	14.58 θ	11.84 θ	11.73 θ	9.69 θ	11.13 θ	11.01 θ	8.70 θ
25.60 y	25.54 y	23.45 y	21.58 y	21.53 y	19.31 y	14.93 y	14.89 y	12.34 y
32.07 x	32.01 x	25.95 x	28.99 x	28.92 x	22.77 x	24.98 x	24.91 x	17.79 x
38.85 y	38.66 y	36.81 y	37.56 y	37.37 y	34.18 θ	28.78 θ	28.41 θ	21.56 θ
45.17 θ	44.64 θ	40.65 θ	38.75 θ	38.28 θ	35.29 y	36.28 y	36.06 y	34.79 y
48.37 y	48.01 y	42.21 x	47.57 x	47.34 x	40.66 x	41.65 y	41.35 y	38.75 y
48.68 x	48.44 x	46.98 y	48.19 y	47.83 y	46.73 y	47.06 x	46.79 x	40.62 x
60.60 x	60.15 x	56.74 x	60.45 x	59.99 x	56.38 x	54.76 x	54.34 x	49.47 x
68.64 θ	67.48 θ	62.96 θ	66.46 θ	65.31 θ	60.43 θ	64.86 θ	63.64 θ	59.98 θ
85.51 θ	83.62 θ	81.05 θ	85.20 θ	83.31 θ	80.53 θ	74.27 θ	72.61 θ	68.57 θ

Table 2: Natural frequencies [Hz] of analytical models for Cases 1–3.
Modes with weak direction dominant motion are shaded.

Element		*Undamaged*	*Damage Pattern*					
Story	*DOF*		*(i)*	*(ii)*	*(iii)*	*(iv)*	*(v)*	*(vi)*
1	x	106.60	58.37	58.37	106.60	106.60	106.60	106.60
1	y	67.90	19.67	19.67	55.85	55.85	55.85	63.89
1	θ	232.02	81.30	81.30	209.11	209.11	209.11	225.35
2	x	106.60	106.60	106.60	106.60	106.60	106.60	106.60
2	y	67.90	67.90	67.90	67.90	67.90	67.90	67.90
2	θ	232.02	232.02	232.02	232.02	232.02	232.02	232.02
3	x	106.60	106.60	58.37	106.60	94.54	94.54	106.60
3	y	67.90	67.90	19.67	67.90	67.90	67.90	67.90
3	θ	232.02	232.02	81.30	232.02	210.78	210.78	232.02
4	x	106.60	106.60	106.60	106.60	106.60	106.60	106.60
4	y	67.90	67.90	67.90	67.90	67.90	67.90	67.90
4	θ	232.02	232.02	232.02	232.02	232.02	232.02	232.02

Table 3: Horizontal story stiffnesses [MN/m] of undamaged and damaged 12DOF model.

Element		*Damage Pattern*					
Story	*DOF*	*(i)*	*(ii)*	*(iii)*	*(iv)*	*(v)*	*(vi)*
1	x	45.24%	45.24%	0	0	0	0
1	y	71.03%	71.03%	17.76%	17.76%	17.76%	5.92%
1	θ	64.96%	64.96%	9.87%	9.87%	9.87%	2.88%
2	x	0	0	0	0	0	0
2	y	0	0	0	0	0	0
2	θ	0	0	0	0	0	0
3	x	0	45.24%	0	11.31%	11.31%	0
3	y	0	71.03%	0	0	0	0
3	θ	0	64.96%	0	9.16%	9.16%	0
4	x	0	0	0	0	0	0
4	y	0	0	0	0	0	0
4	θ	0	0	0	0	0	0

Table 4: Percent loss in horizontal story stiffnesses of damaged 12DOF model.

Undamaged	*Damage Patterns*					
	(i)	*(ii)*	*(iii)*	*(iv)*	*(v)*	*(vi)*
9.29 y	6.18 y	5.76 y	8.79 y	8.79 y	8.79 y	9.15 y
11.64 x	9.80 x	9.39 x	11.64 x	11.50 x	11.50 x	11.64 x
16.19 θ	11.63 θ	10.90 θ	15.80 θ	15.68 θ	15.68 θ	16.07 θ
25.27 y	21.27 y	14.78 y	24.37 y	24.36 y	24.36 y	24.98 y
31.66 x	28.59 x	24.70 x	31.66 x	30.82 x	30.82 x	31.66 x
38.26 y	36.87 y	28.22 θ	37.77 y	37.76 y	37.76 y	38.10 y
44.20 θ	37.93 θ	35.97 y	43.61 θ	42.91 θ	42.91 θ	43.99 θ
47.75 y	46.81 x	40.60 y	47.68 y	47.68 y	47.68 y	47.72 y
47.97 x	47.54 y	46.46 x	47.96 x	47.96 x	47.96 x	47.97 x
59.81 x	59.63 x	53.68 x	59.81 x	58.18 x	58.18 x	59.81 x
66.90 θ	64.67 θ	63.44 θ	66.58 θ	66.56 θ	66.56 θ	66.79 θ
83.23 θ	82.89 θ	71.58 θ	83.18 θ	81.76 θ	81.76 θ	83.21 θ

Table 5: Natural frequencies [Hz] of the 12DOF model with asymmetric mass for Case 4.

Undamaged	*Damage Patterns*					
	(i)	*(ii)*	*(iii)*	*(iv)*	*(v)*	*(vi)*
8.47 y	5.42 y	4.90 y	7.99 y	7.99 y	7.95 y	8.34 y
9.05 x	7.28 x	6.59 x	9.05 x	8.81 x	8.81 x	9.05 x
14.40 θ	9.61 θ	8.60 θ	14.01 θ	13.85 θ	13.85 θ	14.29 θ
23.19 y	19.06 y	12.26 y	22.25 y	22.22 y	22.20 y	22.90 y
25.63 x	22.47 x	17.65 x	25.63 x	24.72 x	24.72 x	25.63 x
36.44 y	33.73 θ	21.44 θ	35.81 y	35.78 y	35.77 y	36.25 y
40.21 θ	34.94 y	34.62 y	39.68 θ	38.84 θ	38.84 θ	40.01 θ
41.85 x	40.23 x	38.17 y	41.84 x	41.71 x	41.71 x	41.85 x
46.77 y	46.50 y	40.13 x	46.68 y	46.68 y	46.66 y	46.74 y
56.55 x	56.17 x	49.20 x	56.55 x	54.67 x	54.67 x	56.55 x
62.42 θ	59.82 θ	59.58 θ	62.04 θ	62.04 θ	62.04 θ	62.29 θ
80.75 θ	80.20 θ	67.85 θ	80.67 θ	79.07 θ	79.07 θ	80.72 θ

Table 6: Natural frequencies [Hz] of the 120DOF model with asymmetric mass for Cases 5–6.

Element		*Undamaged*	*Damage Pattern*					
Story	*DOF*		*(i)*	*(ii)*	*(iii)*	*(iv)*	*(v)*	*(vi)*
1	x	77.38	35.21	35.49	77.38	77.47	77.47	77.38
1	y	61.62	15.41	15.54	49.82	49.82	49.07	57.74
1	θ	197.34	56.05	56.98	179.33	179.43	179.42	191.41
2	x	57.38	49.05	43.35	57.38	56.16	56.16	57.38
2	y	53.66	46.57	42.90	52.95	52.94	52.18	53.47
2	θ	171.75	142.54	126.22	169.99	168.78	168.77	171.29
3	x	54.88	54.85	22.17	54.87	46.54	46.54	54.88
3	y	51.04	51.13	12.25	51.05	51.03	51.08	51.04
3	θ	174.97	178.95	41.00	175.17	156.83	156.83	175.02
4	x	52.85	52.44	42.22	52.84	51.14	51.14	52.85
4	y	49.16	48.69	41.68	49.12	49.09	49.08	49.15
4	θ	175.93	175.44	135.69	175.91	173.83	173.82	175.92

Table 7: "Equivalent" Horizontal story stiffnesses [MN/m] of 120DOF model.

Element		*Damage Pattern*					
Story	*DOF*	*(i)*	*(ii)*	*(iii)*	*(iv)*	*(v)*	*(vi)*
1	x	54.50%	54.13%	–0.00%	–0.11%	–0.11%	0
1	y	74.99%	74.79%	19.14%	19.15%	20.38%	6.29%
1	θ	71.60%	71.12%	9.12%	9.08%	9.08%	3.00%
2	x	14.52%	24.44%	0	2.13%	2.13%	0
2	y	13.21%	20.06%	1.32%	1.34%	2.75%	0.35%
2	θ	17.00%	26.51%	1.02%	1.73%	1.73%	0.27%
3	x	0.04%	59.61%	0.01%	15.20%	15.20%	0
3	y	–0.19%	76.00%	–0.02%	0.02%	–0.08%	0
3	θ	–2.27%	76.56%	–0.11%	10.37%	10.36%	–0.03%
4	x	0.76%	20.10%	0.01%	3.23%	3.23%	0
4	y	0.95%	15.23%	0.08%	0.14%	0.17%	0.02%
4	θ	0.28%	22.87%	0.01%	1.19%	1.20%	0

Table 8: Percent loss in "equivalent" horizontal story stiffnesses of damaged 120DOF model.

Description	*Case 1* (1D+noise) (weak dir.)	*Case 2* (+ model error)	*Case 3* (roof excit)	*Case 4* (3D)	*Case 5* (+ model error)	*Case 6* (+ limited sensors)
Data generation model:						
1. Floors rigid (USC 12DOF)	×		×	×		
2. Floors rigid in-plane (HKUST 120DOF)		×			×	×
Mass Distribution:						
1. Symmetric (four 400kg masses on roof)	×	×	×			
2. Asymmetric (three 400kg, one 550 kg)				×	×	×
Excitation:						
1. "Ambient"	×	×				
2. Shaker diagonal on roof			×	×	×	×
ID Model: linear 12DOF shear building	×	×	×	×	×	×
ID Data: 4 sensors/floor with 10% RMS noise						
1. Known input	a	a				
2. Unknown input	b	b	b	b	b	
3. Unknown input; sensors on 2^{nd},4^{th} floors						c
Damage Patterns: remove the following						
i. all braces in 1^{st} story	×	×	×	×	×	×
ii. all braces in 1^{st} and 3^{rd} stories	×	×	×	×	×	×
iii. one brace in 1^{st} story				×	×	×
iv. one brace in each of 1^{st} and 3^{rd} stories				×	×	×
v. as *iv*, and loosen floor beam at 1^{st} level					×	×
vi. 2/3 stiffness in one brace in at 1^{st} story				×	×	×

Table 9: Simulation case matrix of the phase 1 SHM benchmark problem.

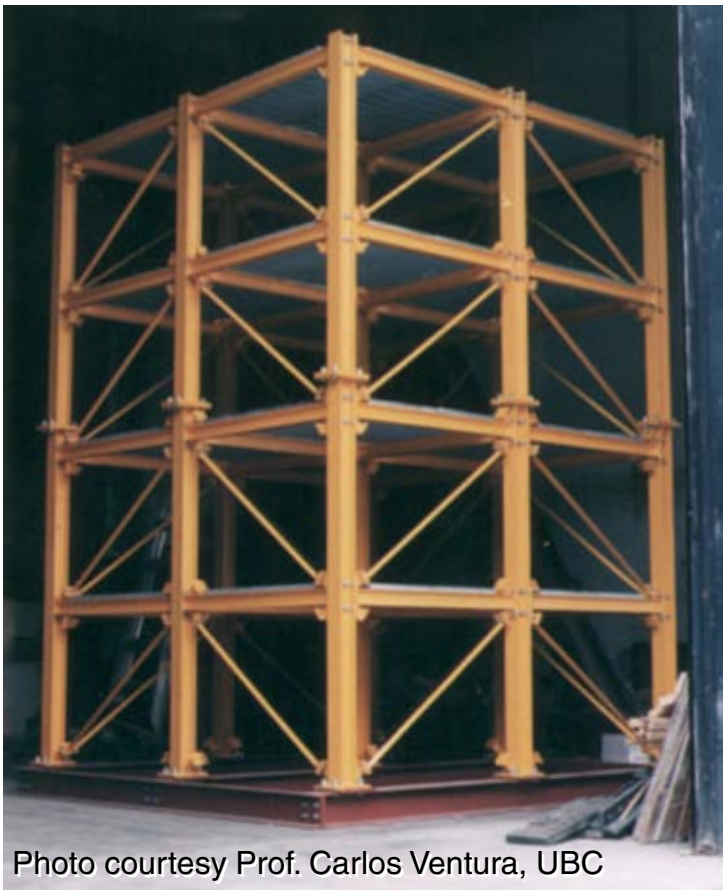

Figure 1: Steel-frame scale structure.

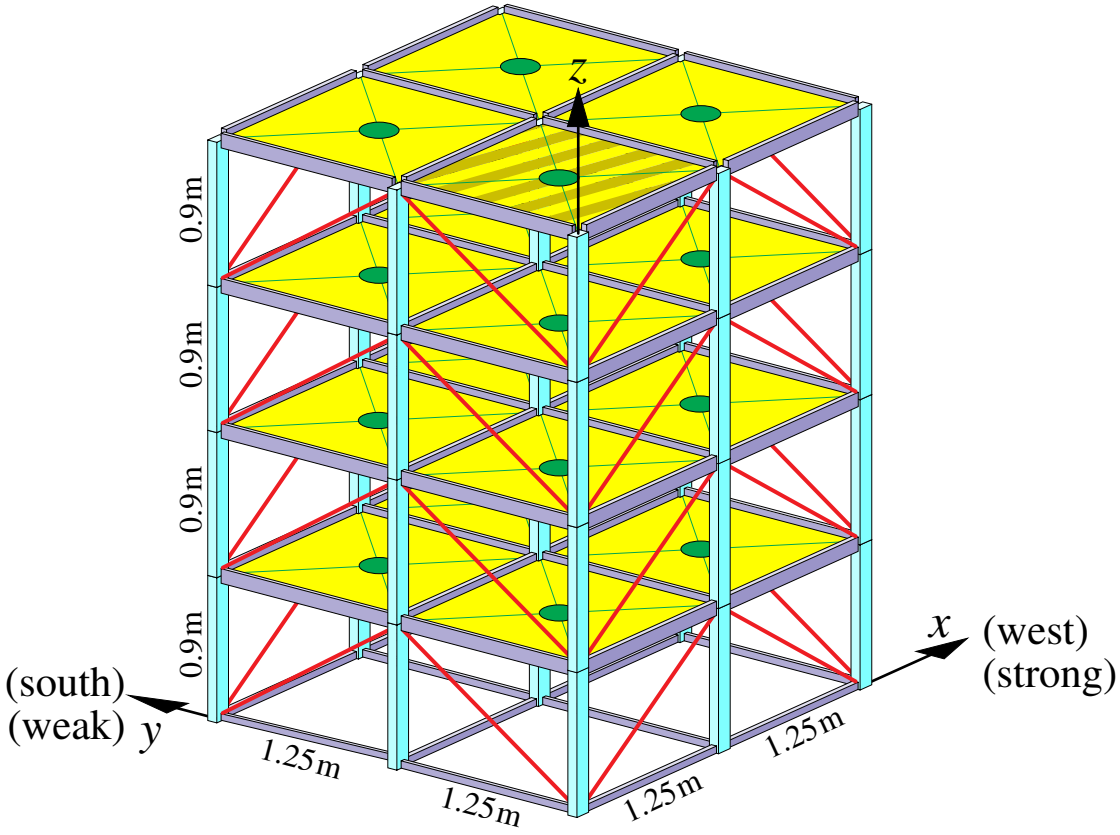

Figure 2: Diagram of analytical model with strong and weak directions as shown.

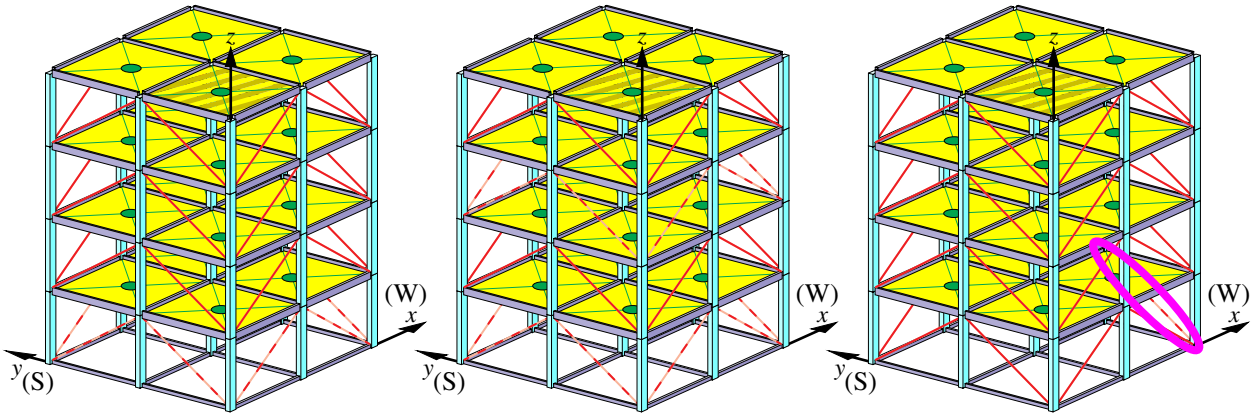

(*i*) no stiffness in 1st floor braces

(*ii*) no stiffness in 1st floor braces
no stiffness in 3rd floor braces

(*iii*) no stiffness in one 1st floor brace

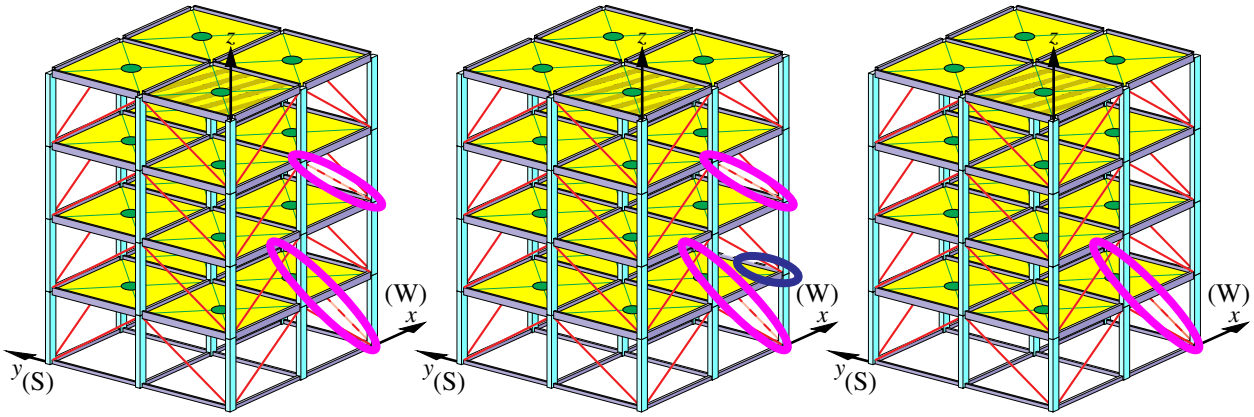

(*iv*) no stiffness in one 1st floor brace
no stiffness in one 3rd floor brace

(*v*) no stiffness in one 1st floor brace
no stiffness in one 3rd floor brace
beam-column connection weakened

(*vi*) $^{2}/_{3}$ stiffness in one 1st floor brace

Figure 3: The six damage patterns.

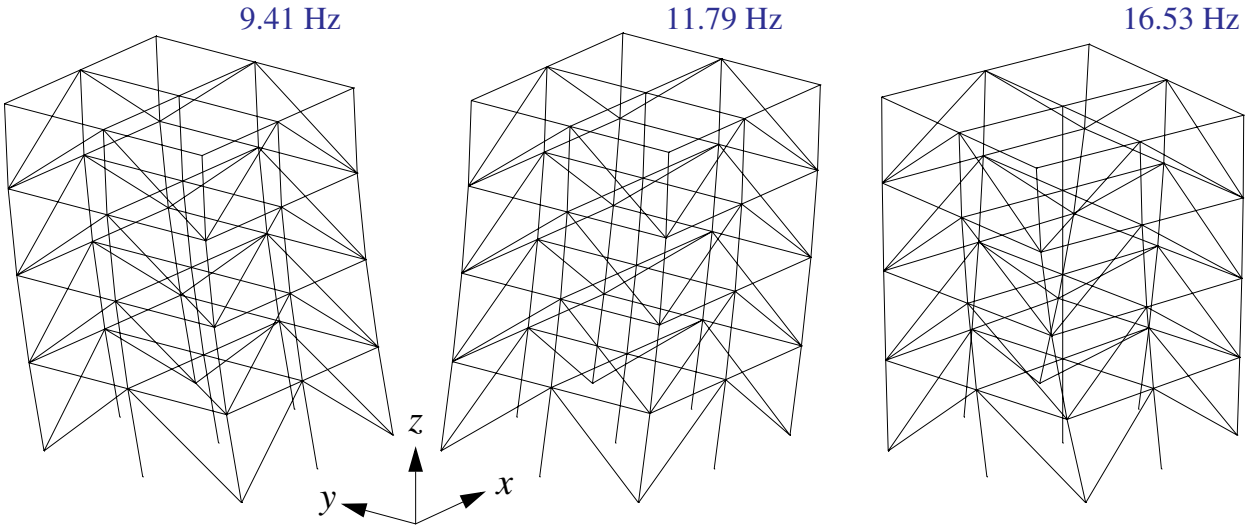

Figure 4: First 3 mode shapes of the 12DOF consistent-mass-matrix model.

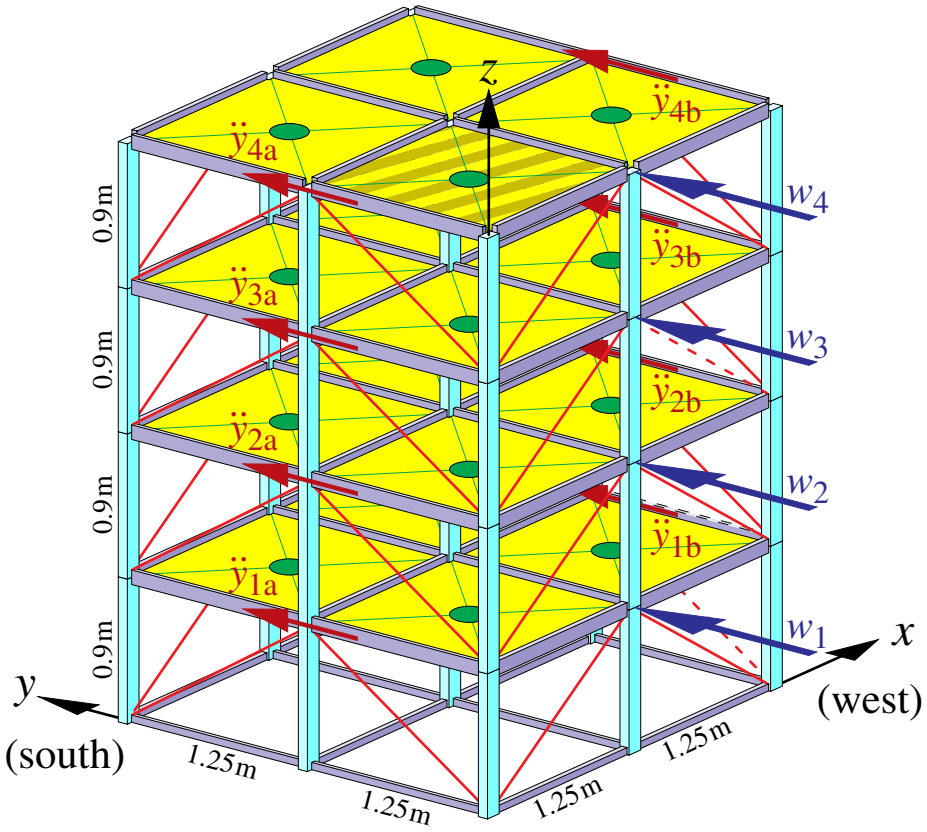

Figure 5: Diagram of model for Cases 1–2.
Note: The w_i are excitations and the $\ddot{y}_{ij}$ are accelerometer measurements (the $\ddot{y}_{ic}$ and $\ddot{y}_{id}$ in the *x*-direction are omitted for clarity).

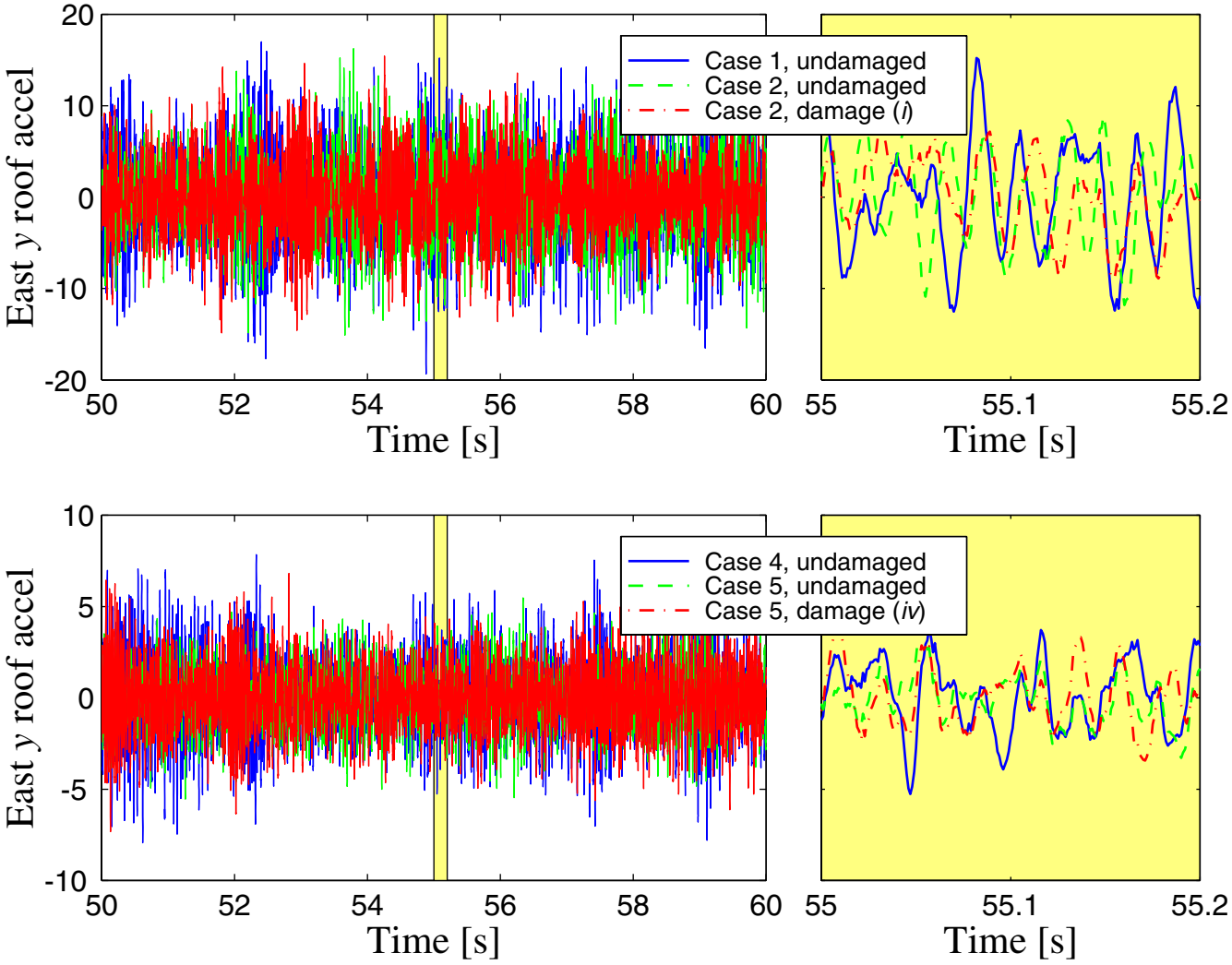

Figure 6: Typical acceleration time histories for several cases and damage patterns.
The plots on the right are a blow-up of the little strip near the center of the left-hand plots.

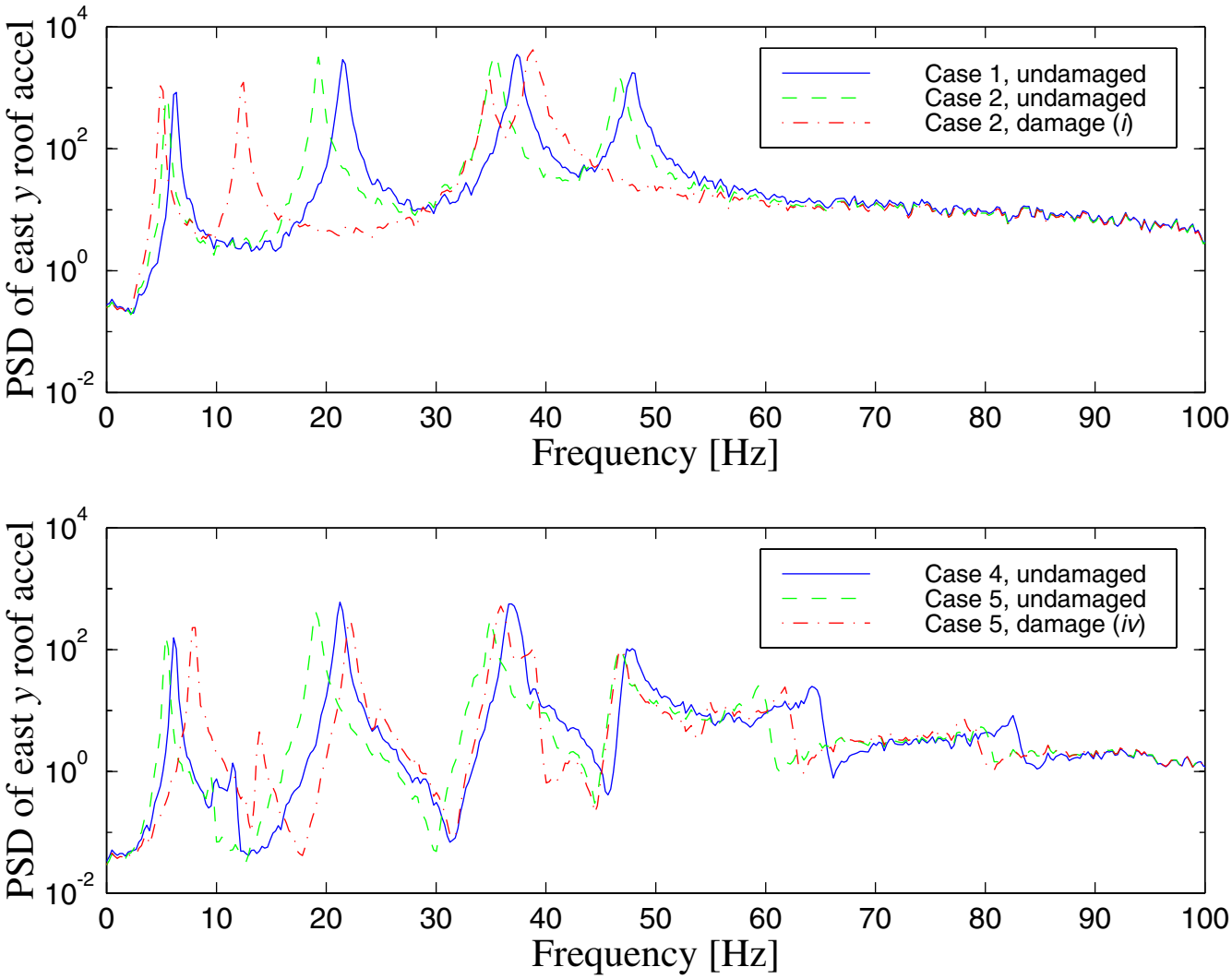

Figure 7: Typical acceleration power spectral densities for several cases and damage patterns.

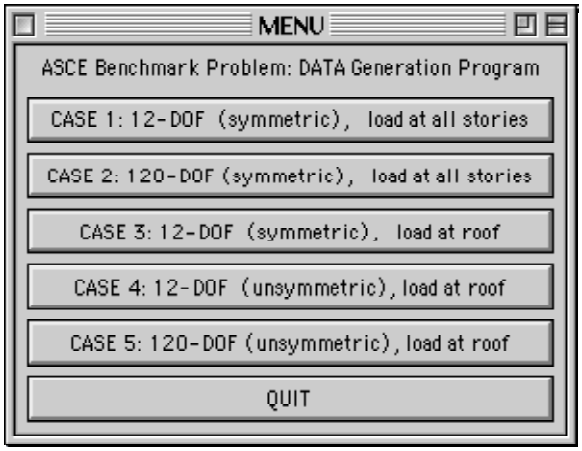

(*a*) **startup GUI to select the analysis case.**

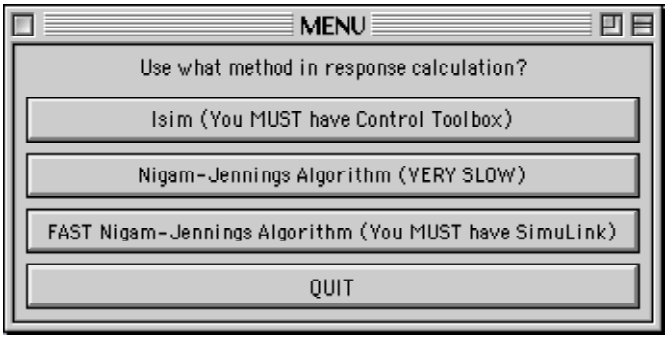

(*c*) **GUI to select the integration routine.**

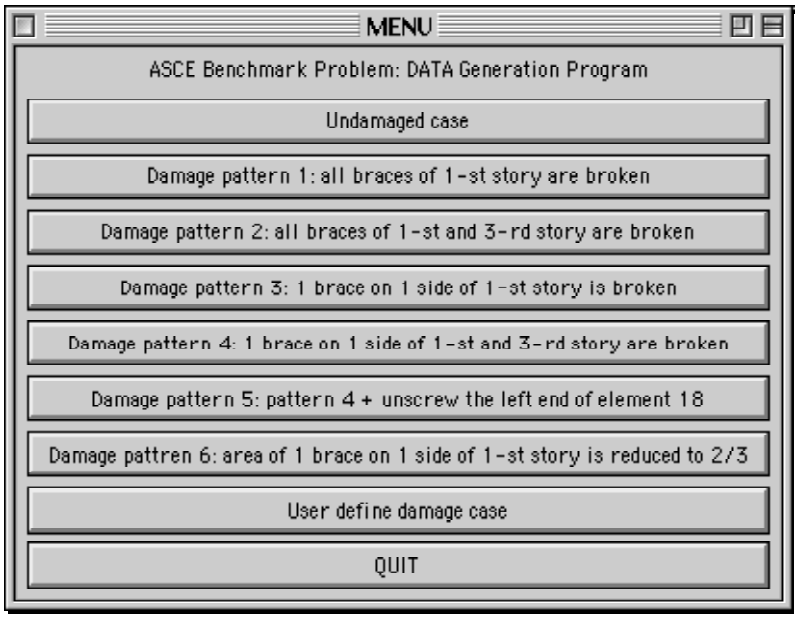

(*b*) **GUI to select the damage pattern.**

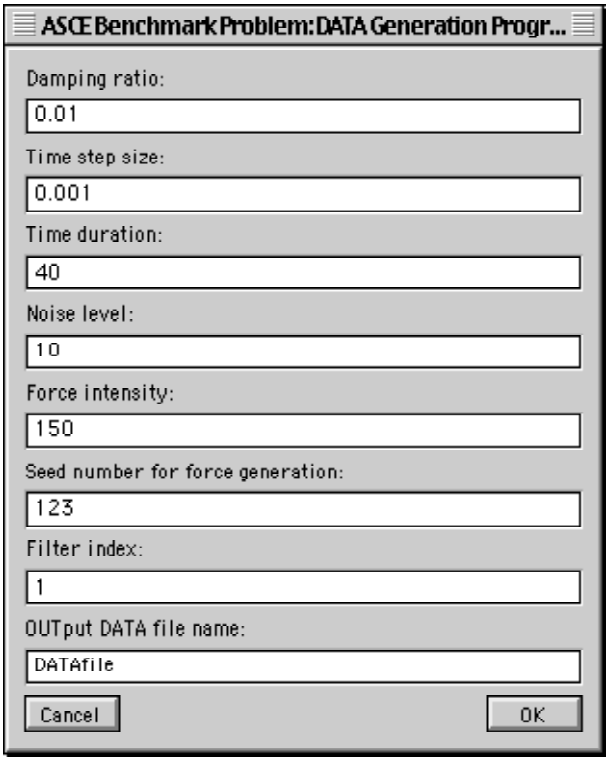

(*d*) **GUI to enter the numerical quantities.**

Figure 8: *datagen*'s standard graphical user interface.

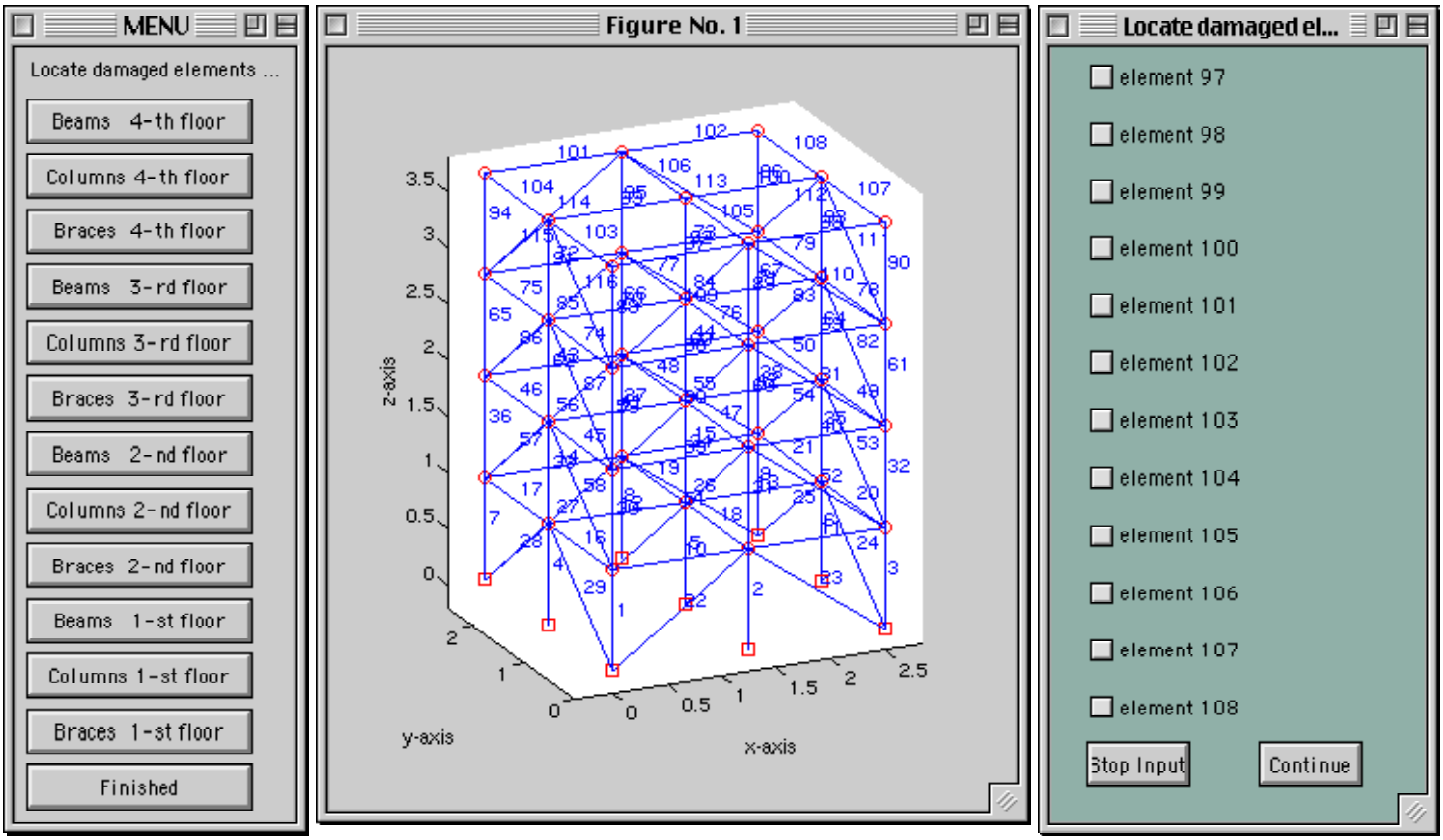

(*a*) Element categories. (*b*) Frame drawing of the elements. (*c*) Specific elements.

Figure 9: *datagen*'s graphical user interface for user-selectable damage patterns.

$$\mathbf{M}^{\text{undamaged}}_{\substack{\text{12DOF}\\\text{consistent}\\\text{Case 1}}} = \begin{bmatrix}
3430.2 & 0 & 0 & 11.1 & 0 & 0 & 0 & 0 & 0 & 0 & 0 & 0 \\
0 & 3430.2 & 0 & 0 & 11.1 & 0 & 0 & 0 & 0 & 0 & 0 & 0 \\
0 & 0 & 3726.4 & 0 & 0 & 23.0 & 0 & 0 & 0 & 0 & 0 & 0 \\
11.1 & 0 & 0 & 2630.2 & 0 & 0 & 11.1 & 0 & 0 & 0 & 0 & 0 \\
0 & 11.1 & 0 & 0 & 2630.2 & 0 & 0 & 11.1 & 0 & 0 & 0 & 0 \\
0 & 0 & 23.0 & 0 & 0 & 2893.0 & 0 & 0 & 23.0 & 0 & 0 & 0 \\
0 & 0 & 0 & 11.1 & 0 & 0 & 2630.2 & 0 & 0 & 11.1 & 0 & 0 \\
0 & 0 & 0 & 0 & 11.1 & 0 & 0 & 2630.2 & 0 & 0 & 11.1 & 0 \\
0 & 0 & 0 & 0 & 0 & 23.0 & 0 & 0 & 2893.0 & 0 & 0 & 23.0 \\
0 & 0 & 0 & 0 & 0 & 0 & 11.1 & 0 & 0 & 1798.8 & 0 & 0 \\
0 & 0 & 0 & 0 & 0 & 0 & 0 & 11.1 & 0 & 0 & 1798.8 & 0 \\
0 & 0 & 0 & 0 & 0 & 0 & 0 & 0 & 23.0 & 0 & 0 & 1991.1
\end{bmatrix} \text{ kg}$$

$$\mathbf{M}^{(i)}_{\substack{\text{12DOF}\\\text{consistent}\\\text{Case 1}}} = \begin{bmatrix}
3425.3 & 0 & 0 & 11.1 & 0 & 0 & 0 & 0 & 0 & 0 & 0 & 0 \\
0 & 3425.3 & 0 & 0 & 11.1 & 0 & 0 & 0 & 0 & 0 & 0 & 0 \\
0 & 0 & 3718.8 & 0 & 0 & 23.0 & 0 & 0 & 0 & 0 & 0 & 0 \\
11.1 & 0 & 0 & 2630.2 & 0 & 0 & 11.1 & 0 & 0 & 0 & 0 & 0 \\
0 & 11.1 & 0 & 0 & 2630.2 & 0 & 0 & 11.1 & 0 & 0 & 0 & 0 \\
0 & 0 & 23.0 & 0 & 0 & 2893.0 & 0 & 0 & 23.0 & 0 & 0 & 0 \\
0 & 0 & 0 & 11.1 & 0 & 0 & 2630.2 & 0 & 0 & 11.1 & 0 & 0 \\
0 & 0 & 0 & 0 & 11.1 & 0 & 0 & 2630.2 & 0 & 0 & 11.1 & 0 \\
0 & 0 & 0 & 0 & 0 & 23.0 & 0 & 0 & 2893.0 & 0 & 0 & 23.0 \\
0 & 0 & 0 & 0 & 0 & 0 & 11.1 & 0 & 0 & 1798.8 & 0 & 0 \\
0 & 0 & 0 & 0 & 0 & 0 & 0 & 11.1 & 0 & 0 & 1798.8 & 0 \\
0 & 0 & 0 & 0 & 0 & 0 & 0 & 0 & 23.0 & 0 & 0 & 1991.1
\end{bmatrix} \text{ kg}$$

$$\mathbf{M}^{(ii)}_{\substack{\text{12DOF}\\\text{consistent}\\\text{Case 1}}} = \begin{bmatrix}
3425.3 & 0 & 0 & 11.1 & 0 & 0 & 0 & 0 & 0 & 0 & 0 & 0 \\
0 & 3425.3 & 0 & 0 & 11.1 & 0 & 0 & 0 & 0 & 0 & 0 & 0 \\
0 & 0 & 3718.8 & 0 & 0 & 23.0 & 0 & 0 & 0 & 0 & 0 & 0 \\
11.1 & 0 & 0 & 2625.3 & 0 & 0 & 9.2 & 0 & 0 & 0 & 0 & 0 \\
0 & 11.1 & 0 & 0 & 2625.3 & 0 & 0 & 9.2 & 0 & 0 & 0 & 0 \\
0 & 0 & 23.0 & 0 & 0 & 2879.9 & 0 & 0 & 19.2 & 0 & 0 & 0 \\
0 & 0 & 0 & 9.2 & 0 & 0 & 2625.3 & 0 & 0 & 11.1 & 0 & 0 \\
0 & 0 & 0 & 0 & 9.2 & 0 & 0 & 2625.3 & 0 & 0 & 11.1 & 0 \\
0 & 0 & 0 & 0 & 0 & 19.2 & 0 & 0 & 2885.5 & 0 & 0 & 23.0 \\
0 & 0 & 0 & 0 & 0 & 0 & 11.1 & 0 & 0 & 1798.8 & 0 & 0 \\
0 & 0 & 0 & 0 & 0 & 0 & 0 & 11.1 & 0 & 0 & 1798.8 & 0 \\
0 & 0 & 0 & 0 & 0 & 0 & 0 & 0 & 23.0 & 0 & 0 & 1991.1
\end{bmatrix} \text{ kg}$$

$$\mathbf{M}^{\text{all patterns}}_{\substack{\text{12DOF}\\\text{lumped}\\\text{Cases 1\&3}}} = \begin{bmatrix}
3452.4 & 0 & 0 & 0 & 0 & 0 & 0 & 0 & 0 & 0 & 0 & 0 \\
0 & 3452.4 & 0 & 0 & 0 & 0 & 0 & 0 & 0 & 0 & 0 & 0 \\
0 & 0 & 3819.4 & 0 & 0 & 0 & 0 & 0 & 0 & 0 & 0 & 0 \\
0 & 0 & 0 & 2652.4 & 0 & 0 & 0 & 0 & 0 & 0 & 0 & 0 \\
0 & 0 & 0 & 0 & 2652.4 & 0 & 0 & 0 & 0 & 0 & 0 & 0 \\
0 & 0 & 0 & 0 & 0 & 2986.1 & 0 & 0 & 0 & 0 & 0 & 0 \\
0 & 0 & 0 & 0 & 0 & 0 & 2652.4 & 0 & 0 & 0 & 0 & 0 \\
0 & 0 & 0 & 0 & 0 & 0 & 0 & 2652.4 & 0 & 0 & 0 & 0 \\
0 & 0 & 0 & 0 & 0 & 0 & 0 & 0 & 2986.1 & 0 & 0 & 0 \\
0 & 0 & 0 & 0 & 0 & 0 & 0 & 0 & 0 & 1809.9 & 0 & 0 \\
0 & 0 & 0 & 0 & 0 & 0 & 0 & 0 & 0 & 0 & 1809.9 & 0 \\
0 & 0 & 0 & 0 & 0 & 0 & 0 & 0 & 0 & 0 & 0 & 2056.9
\end{bmatrix} \text{ kg}$$

$$\mathbf{M}^{\text{all patterns}}_{\substack{\text{12DOF}\\\text{lumped}\\\text{Case 4}}} = \begin{bmatrix}
3452.4 & 0 & 0 & 0 & 0 & 0 & 0 & 0 & 0 & 0 & 0 & 0 \\
0 & 3452.4 & 0 & 0 & 0 & 0 & 0 & 0 & 0 & 0 & 0 & 0 \\
0 & 0 & 3819.4 & 0 & 0 & 0 & 0 & 0 & 0 & 0 & 0 & 0 \\
0 & 0 & 0 & 2652.4 & 0 & 0 & 0 & 0 & 0 & 0 & 0 & 0 \\
0 & 0 & 0 & 0 & 2652.4 & 0 & 0 & 0 & 0 & 0 & 0 & 0 \\
0 & 0 & 0 & 0 & 0 & 2986.1 & 0 & 0 & 0 & 0 & 0 & 0 \\
0 & 0 & 0 & 0 & 0 & 0 & 2652.4 & 0 & 0 & 0 & 0 & 0 \\
0 & 0 & 0 & 0 & 0 & 0 & 0 & 2652.4 & 0 & 0 & 0 & 0 \\
0 & 0 & 0 & 0 & 0 & 0 & 0 & 0 & 2986.1 & 0 & 0 & 0 \\
0 & 0 & 0 & 0 & 0 & 0 & 0 & 0 & 0 & 1959.9 & 0 & 93.8 \\
0 & 0 & 0 & 0 & 0 & 0 & 0 & 0 & 0 & 0 & 1959.9 & -93.8 \\
0 & 0 & 0 & 0 & 0 & 0 & 0 & 0 & 0 & 93.8 & -93.8 & 2213.1
\end{bmatrix} \text{ kg}$$

Figure 10: Mass matrices of the 12DOF models.

Note: zero elements are light green (light gray); medium blue (medium gray) denotes elements of the damaged consistent mass matrices elements unchanged from the undamaged, and of the Case 4 lumped mass matrix elements unchanged from the corresponding Cases 1&3 matrix.

$$\mathbf{K}_{12\text{DOF}}^{\text{undamaged}} = \begin{bmatrix} 213.20 & 0 & 0 & -106.60 & 0 & 0 & 0 & 0 & 0 & 0 & 0 & 0 \\ 0 & 135.81 & 0 & 0 & -67.90 & 0 & 0 & 0 & 0 & 0 & 0 & 0 \\ 0 & 0 & 464.04 & 0 & 0 & -232.02 & 0 & 0 & 0 & 0 & 0 & 0 \\ -106.60 & 0 & 0 & 213.20 & 0 & 0 & -106.60 & 0 & 0 & 0 & 0 & 0 \\ 0 & -67.90 & 0 & 0 & 135.81 & 0 & 0 & -67.90 & 0 & 0 & 0 & 0 \\ 0 & 0 & -232.02 & 0 & 0 & 464.04 & 0 & 0 & -232.02 & 0 & 0 & 0 \\ 0 & 0 & 0 & -106.60 & 0 & 0 & 213.20 & 0 & 0 & -106.60 & 0 & 0 \\ 0 & 0 & 0 & 0 & -67.90 & 0 & 0 & 135.81 & 0 & 0 & -67.90 & 0 \\ 0 & 0 & 0 & 0 & 0 & -232.02 & 0 & 0 & 464.04 & 0 & 0 & -232.02 \\ 0 & 0 & 0 & 0 & 0 & 0 & -106.60 & 0 & 0 & 106.60 & 0 & 0 \\ 0 & 0 & 0 & 0 & 0 & 0 & 0 & -67.90 & 0 & 0 & 67.90 & 0 \\ 0 & 0 & 0 & 0 & 0 & 0 & 0 & 0 & -232.02 & 0 & 0 & 232.02 \end{bmatrix} \frac{\text{MN}}{\text{m}}$$

$$\mathbf{K}_{12\text{DOF}}^{(i)} = \begin{bmatrix} 164.97 & 0 & 0 & -106.60 & 0 & 0 & 0 & 0 & 0 & 0 & 0 & 0 \\ 0 & 87.58 & 0 & 0 & -67.90 & 0 & 0 & 0 & 0 & 0 & 0 & 0 \\ 0 & 0 & 313.32 & 0 & 0 & -232.02 & 0 & 0 & 0 & 0 & 0 & 0 \\ -106.60 & 0 & 0 & 213.20 & 0 & 0 & -106.60 & 0 & 0 & 0 & 0 & 0 \\ 0 & -67.90 & 0 & 0 & 135.81 & 0 & 0 & -67.90 & 0 & 0 & 0 & 0 \\ 0 & 0 & -232.02 & 0 & 0 & 464.04 & 0 & 0 & -232.02 & 0 & 0 & 0 \\ 0 & 0 & 0 & -106.60 & 0 & 0 & 213.20 & 0 & 0 & -106.60 & 0 & 0 \\ 0 & 0 & 0 & 0 & -67.90 & 0 & 0 & 135.81 & 0 & 0 & -67.90 & 0 \\ 0 & 0 & 0 & 0 & 0 & -232.02 & 0 & 0 & 464.04 & 0 & 0 & -232.02 \\ 0 & 0 & 0 & 0 & 0 & 0 & -106.60 & 0 & 0 & 106.60 & 0 & 0 \\ 0 & 0 & 0 & 0 & 0 & 0 & 0 & -67.90 & 0 & 0 & 67.90 & 0 \\ 0 & 0 & 0 & 0 & 0 & 0 & 0 & 0 & -232.02 & 0 & 0 & 232.02 \end{bmatrix} \frac{\text{MN}}{\text{m}}$$

$$\mathbf{K}_{12\text{DOF}}^{(ii)} = \begin{bmatrix} 164.97 & 0 & 0 & -106.60 & 0 & 0 & 0 & 0 & 0 & 0 & 0 & 0 \\ 0 & 87.58 & 0 & 0 & -67.90 & 0 & 0 & 0 & 0 & 0 & 0 & 0 \\ 0 & 0 & 313.32 & 0 & 0 & -232.02 & 0 & 0 & 0 & 0 & 0 & 0 \\ -106.60 & 0 & 0 & 164.97 & 0 & 0 & -58.37 & 0 & 0 & 0 & 0 & 0 \\ 0 & -67.90 & 0 & 0 & 87.58 & 0 & 0 & -19.67 & 0 & 0 & 0 & 0 \\ 0 & 0 & -232.02 & 0 & 0 & 313.32 & 0 & 0 & -81.30 & 0 & 0 & 0 \\ 0 & 0 & 0 & -58.37 & 0 & 0 & 164.97 & 0 & 0 & -106.60 & 0 & 0 \\ 0 & 0 & 0 & 0 & -19.67 & 0 & 0 & 87.58 & 0 & 0 & -67.90 & 0 \\ 0 & 0 & 0 & 0 & 0 & -81.30 & 0 & 0 & 313.32 & 0 & 0 & -232.02 \\ 0 & 0 & 0 & 0 & 0 & 0 & -106.60 & 0 & 0 & 106.60 & 0 & 0 \\ 0 & 0 & 0 & 0 & 0 & 0 & 0 & -67.90 & 0 & 0 & 67.90 & 0 \\ 0 & 0 & 0 & 0 & 0 & 0 & 0 & 0 & -232.02 & 0 & 0 & 232.02 \end{bmatrix} \frac{\text{MN}}{\text{m}}$$

$$\mathbf{K}_{12\text{DOF}}^{(iii)} = \begin{bmatrix} 213.20 & 0 & 0 & -106.60 & 0 & 0 & 0 & 0 & 0 & 0 & 0 & 0 \\ 0 & 123.75 & -15.07 & 0 & -67.90 & -232.02 & 0 & 0 & 0 & 0 & 0 & 0 \\ 0 & -15.07 & 445.20 & 0 & 0 & 0 & -106.60 & 0 & 0 & 0 & 0 & 0 \\ -106.60 & 0 & 0 & 213.20 & 0 & 0 & 0 & -67.90 & 0 & 0 & 0 & 0 \\ 0 & -67.90 & 0 & 0 & 135.81 & 0 & 0 & 0 & -232.02 & 0 & 0 & 0 \\ 0 & 0 & -232.02 & 0 & 0 & 464.04 & 0 & 0 & 0 & -106.60 & 0 & 0 \\ 0 & 0 & 0 & -106.60 & 0 & 0 & 213.20 & 0 & 0 & 0 & -67.90 & 0 \\ 0 & 0 & 0 & 0 & -67.90 & 0 & 0 & 135.81 & 0 & 0 & 0 & -232.02 \\ 0 & 0 & 0 & 0 & 0 & -232.02 & 0 & 0 & 464.04 & 0 & 0 & 0 \\ 0 & 0 & 0 & 0 & 0 & 0 & -106.60 & 0 & 0 & 106.60 & 0 & 0 \\ 0 & 0 & 0 & 0 & 0 & 0 & 0 & -67.90 & 0 & 0 & 67.90 & 0 \\ 0 & 0 & 0 & 0 & 0 & 0 & 0 & 0 & -232.02 & 0 & 0 & 232.02 \end{bmatrix} \frac{\text{MN}}{\text{m}}$$

$$\mathbf{K}_{12\text{DOF}}^{(iv)} = \begin{bmatrix} 213.20 & 0 & 0 & -106.60 & 0 & 0 & 0 & 0 & 0 & 0 & 0 & 0 \\ 0 & 123.75 & -15.07 & 0 & -67.90 & -232.02 & 0 & 0 & 0 & 0 & 0 & 0 \\ 0 & -15.07 & 445.20 & 0 & 0 & -15.07 & -94.54 & 0 & 0 & 0 & 0 & 0 \\ -106.60 & 0 & 0 & 201.14 & 0 & 445.20 & 15.07 & -67.90 & 15.07 & 0 & 0 & 0 \\ 0 & -67.90 & 0 & -15.07 & 135.81 & 15.07 & 201.14 & 0 & -213.18 & -106.60 & 0 & 0 \\ 0 & 0 & -232.02 & -94.54 & 0 & -213.18 & -15.07 & 135.81 & -15.07 & 0 & -67.90 & 0 \\ 0 & 0 & 0 & 15.07 & -67.90 & 0 & -106.60 & 0 & 445.20 & 106.60 & 0 & -232.02 \\ 0 & 0 & 0 & 0 & 0 & 0 & 0 & -67.90 & 0 & 0 & 67.90 & 0 \\ 0 & 0 & 0 & 0 & 0 & 0 & 0 & 0 & -232.02 & 0 & 0 & 232.02 \end{bmatrix} \frac{\text{MN}}{\text{m}}$$

$$\mathbf{K}_{12\text{DOF}}^{(v)} = \mathbf{K}_{12\text{DOF}}^{(vi)}$$

$$\mathbf{K}_{12\text{DOF}}^{(vi)} = \begin{bmatrix} 213.20 & 0 & 0 & -106.60 & 0 & 0 & 0 & 0 & 0 & 0 & 0 & 0 \\ 0 & 131.79 & -5.02 & 0 & -67.90 & -232.02 & 0 & 0 & 0 & 0 & 0 & 0 \\ 0 & -5.02 & 457.76 & 0 & 0 & 0 & -106.60 & 0 & 0 & 0 & 0 & 0 \\ -106.60 & 0 & 0 & 213.20 & 0 & 0 & 0 & -67.90 & 0 & 0 & 0 & 0 \\ 0 & -67.90 & 0 & 0 & 135.81 & 0 & 0 & 0 & -232.02 & 0 & 0 & 0 \\ 0 & 0 & -232.02 & 0 & 0 & 464.04 & 0 & 0 & 0 & -106.60 & 0 & 0 \\ 0 & 0 & 0 & -106.60 & 0 & 0 & 213.20 & 0 & 0 & 0 & -67.90 & 0 \\ 0 & 0 & 0 & 0 & -67.90 & 0 & 0 & 135.81 & 0 & 0 & 0 & -232.02 \\ 0 & 0 & 0 & 0 & 0 & -232.02 & 0 & 0 & 464.04 & 0 & 0 & 0 \\ 0 & 0 & 0 & 0 & 0 & 0 & -106.60 & 0 & 0 & 106.60 & 0 & 0 \\ 0 & 0 & 0 & 0 & 0 & 0 & 0 & -67.90 & 0 & 0 & 67.90 & 0 \\ 0 & 0 & 0 & 0 & 0 & 0 & 0 & 0 & -232.02 & 0 & 0 & 232.02 \end{bmatrix} \frac{\text{MN}}{\text{m}}$$

Figure 11: Stiffness matrices of the 12DOF models.

Note: zero elements are light green (light gray); light blue (medium gray) in the damaged cases denote elements that are unchanged from the undamaged stiffness matrix.